Acta Crystallographica Section D
Biological Crystallography
ISSN 0907-4449

Structure of human monocyte chemoattractant protein 4 (MCP-4/CCL13)

Cyril Barinka, Adam Prahl‡ and Jacek Lubkowski*

National Cancer Institute at Frederick, Center for Cancer Research, Frederick, MD 21702, USA

‡ Current address: Laboratory of Organic Synthesis, University of Gdansk, Gdansk, Poland.

Correspondence e-mail: jacek@ncifcrf.gov

Received 19 September 2007
Accepted 7 December 2007

PDB Reference: human monocyte chemoattractant protein 4, 2ra4, r2ra4sf.

Monocyte chemoattractant proteins (MCPs) belong to the CC chemokine family and are involved in many (patho)physiological processes characterized by mononuclear cell infiltration, including tissue remodeling, atherosclerosis and cancer metastasis. Here, the crystal structure of human monocyte chemoattractant protein 4 (MCP-4) refined at 1.70 Å resolution is reported with crystallographic values R = 0.180 and $R_{\rm free}$ = 0.212. The overall MCP-4 fold reveals the typical tertiary features of the CC chemokine family. A central three-stranded antiparallel β-sheet is C-terminally flanked by an overlaying α-helix, while the N-terminal part of the molecule forms an extended loop that is anchored to the rest of the molecule *via* two disulfide bridges, Cys11–Cys35 and Cys12–Cys51. The crystal packing suggests the existence of MCP-4 dimers with a dimerization interface similar to those previously reported for the X-ray structures of MCP-1 and MCP-2.

1. Introduction

Chemokines (chemoattractant cytokines) are small (8–12 kDa) secreted proteins that play an important role in coordinating normal inflammatory responses such as wound repair and tissue remodeling. Additionally, these molecules and their receptors are intimately involved in pathophysiological processes, including neoplastic diseases, arteriosclerosis and allergic inflammation, as well as HIV pathogenesis (Charo & Taubman, 2004; Craig & Loberg, 2006; Luster, 1998; Rollins, 1997; Romagnani, 2002). Not surprisingly, modified chemokines and their small-molecular-weight antagonists/mimetics are being evaluated as candidate molecules for the development of novel therapeutic strategies (Gong *et al.*, 1998; Proudfoot, 2002; Westby & van der Ryst, 2005; Xia & Frangogiannis, 2007).

Most chemokines have four characteristic cysteine residues with Cys^1–Cys^3 and Cys^2–Cys^4 disulfide connectivity. Based on the pattern of their N-terminal cysteines, they can be classified into four major categories: CXC (or α), CC (or β), CX_3C and C chemokines (Zlotnik & Yoshie, 2000). Chemokines exert their biological activity through interactions with seven transmembrane G protein-coupled receptors (GPCRs). Given their structural similarity, many ligands can signal through more than one receptor and many receptors can accommodate various ligands with overlapping specificity (Proudfoot, 2002). This complexity might be further augmented by the propensity of certain chemokines to form unique hetero-oligomers that could modulate the overall signaling response of the receptors (Crown *et al.*, 2006).

Monocyte chemoattractant proteins (MCPs) are members of the CC family of chemokines that share ~60% sequence homology. Four MCPs have been identified in humans and these were recently reclassified as MCP-1 (CCL2), MCP-2 (CCL8), MCP-3 (CCL7) and MCP-4 (CCL13) (Zlotnik & Yoshie, 2000). MCPs can chemoattract monocytes, memory T cells, natural killer cells and eosinophils, mostly by the activation of chemokine receptors CCR1, CCR2, CCR3 and CCR5. Expression of MCPs by endothelial and mononuclear cells and fibroblasts often increases on treatment with pro-inflammatory cytokines and their expression pattern suggests involvement in many human diseases associated with leukocyte recruitment into sites of inflammation or injury (Leach *et al.*, 2007; Proost *et al.*, 1996; Proudfoot, 2002; Rollins, 1997).

The structures of monocyte chemoattractant proteins 1–3 have been solved by both X-ray crystallography and NMR spectroscopy (Blaszczyk *et al.*, 2000; Handel & Domaille, 1996; Kim *et al.*, 1996; Lubkowski *et al.*, 1997; Meunier *et al.*, 1997), revealing features common to monomers of other chemokines. Central to the chemokine monomer fold is a three-stranded antiparallel β-sheet, followed by a C-terminal α-helix packed against the sheet. An extended N-terminal loop, which is anchored to the rest of the protein by Cys^1–Cys^3 and Cys^2–Cys^4 disulfide bonds, is indispensable for biological activity and participates in the formation of dimers or higher oligomers of MCPs (Blaszczyk *et al.*, 2000; Gong & Clark-Lewis, 1995; Lubkowski *et al.*, 1997; Masure *et al.*, 1995). The crystal structure of MCP-4 presented here extends our understanding of the structural features of the CC chemokine family, including the motifs involved in chemokine oligomerization. Furthermore, the data may provide a structural basis for the development of chemokine receptor antagonists/agonists that are selective and therapeutically effective.

Table 1
Data-collection and refinement statistics.

Values in parentheses are for the highest resolution shell.

Data-collection statistics	
Wavelength (Å)	1.00
Space group	*I*4
Unit-cell parameters (Å)	$a = b = 74.7$, $c = 51.6$
Resolution limits (Å)	50.0–1.70 (1.76–1.70)
No. of unique reflections	15683 (1526)
Redundancy	12.7 (5.4)
Completeness (%)	99.9 (99.5)
$I/\sigma(I)$	26.2 (2.6)
$R_{\rm merge}$	0.072 (0.568)
Refinement statistics	
Resolution limits (Å)	30.0–1.70 (1.74–1.70)
Total no. of reflections	14893 (1127)
No. of reflections in working set	14110 (1073)
No. of reflections in test set	783 (54)
$R/R_{\rm free}$	0.179 (0.233)/0.216 (0.286)
Total no. of non-H atoms	1215
No. of ions	7
No. of water molecules	72
Average *B* factor for all atoms (Å^2)	31.7
Average *B* factor for protein atoms (Å^2)	30.2
Ramachandran plot (%)	
Most favored	94.9
Additionally allowed	5.1
Generously allowed	0.0
Disallowed	0.0
R.m.s. deviations	0.020
Bond lengths (Å)	
Bond angles (°)	1.83
Planarity (Å)	0.010
Chiral centers (Å^3)	0.15

2. Materials and methods

2.1. Cloning and expression

The DNA sequence encoding human MCP-4 (amino acids 1–75 of the mature protein preceded by a starting methionine) was derived from previously reported data (Berkhout *et al.*, 1997). The *DNAWorks* program was used to design a set of MCP-4-specific oligonucleotides and the synthetic MCP-4 gene was assembled according to the recommended protocol (Hoover & Lubkowski, 2002). The synthetic gene (for the sequence, see Supplementary Fig. S1[1]) was then cloned into the pET-11d vector (Novagen); the resulting plasmid was designated pET11_MCP4. Large-scale expression in *Escherichia coli* BL21(DE3)*trxB* was carried out according to standard protocols. Briefly, a single bacterial colony [BL21(DE3)*trxB* cells transformed with pET11_MCP4] was expanded in Luria broth medium and protein expression was induced using 1 m*M* isopropyl β-D-1-thiogalactopyranoside (final concentration) at $OD_{600} = 0.8$. Following 4 h incubation at 310 K, the cells were harvested by centrifugation and stored at 193 K until futher use.

2.2. Purification and refolding

The frozen biomass was suspended in lysis buffer (50 m*M* Tris–HCl, 100 m*M* NaCl, 50 m*M* $MgSO_4$ pH 8.0) supplemented with Complete protease-inhibitor cocktail (Roche Molecular Biochemicals, Indianapolis, Indiana, USA) and lysed by two passes through a French press (American Instrument Co.) at 20.1 MPa. The resulting cell lysate was centrifuged at 20 000*g* for 15 min and the supernatant was filtered through a 0.22 µm filter (Corning) and diluted fivefold with distilled water. The sample was then applied onto an SP-Sepharose column (Pharmacia) equilibrated with 20 m*M* Tris–HCl, 10 m*M* NaCl pH 8.0 and MCP-4 was eluted with a gradient of 0–1 *M* NaCl in 20 m*M* Tris–HCl pH 8.0. The fractions containing MCP-4 were pooled, diluted twofold with 100 m*M* Tris–HCl, 0.5 m*M* EDTA pH 8.5 and disulfide-bond formation was aided by stirring the sample at 277 K for 48 h. The final purification of oxidized MCP-4 was performed by preparative reverse-phase HPLC using a C-18 column (YMC-Pack, ODS-AP) and a 5–30% linear concentration gradient of acetonitrile supplemented with 0.1% TFA over 90 min. The final MCP-4 preparation was lyophilized and the protein was dissolved in distilled water at a concentration of 30 mg ml^{-1}.

[1] Supplementary material has been deposited in the IUCr electronic archive (Reference: SX5080). Services for accessing this material are described at the back of the journal.

2.3. Crystallization and diffraction data collection

Initial crystallization conditions were established using the sitting-drop vapor-diffusion method with the MCP-4 protein at a concentration of 30 mg ml^{-1} and a set of commercially available screens from Hampton Research. Optimization of the original conditions yielded diffraction-quality crystals, which were grown at 293 K in hanging drops consisting of a 1:1 mixture of 30 mg ml^{-1} MCP-4 (dissolved in deionized water) and reservoir solution (0.1 *M* bis-tris, 2 *M* ammonium sulfate pH 6.5). Crystals reached final dimensions of approximately 0.3 × 0.3 × 0.2 mm in about four weeks. For data collection, crystals were flash-frozen in liquid nitrogen using the well solution supplemented with 25%(*v*/*v*) glycerol as a cryoprotectant. Diffraction data were collected from a single crystal at 100 K at the Advanced Photon Source (Argonne, Illinois, USA) using the SER-CAT beamline 22-ID equipped with a MAR300 charge-coupled device detector, a crystal-to-detector distance of 200 mm and an X-ray wavelength of 1.00 Å. The images were processed and the data were scaled using the *HKL*-2000 software package (Otwinowski & Minor, 1997); the final statistics are summarized in Table 1.

2.4. Structure determination

The MCP-4 structure was solved by molecular replacement using a monomer of MCP-1 (PDB code 1dok) as the search model in order to locate the orientation and positions of both independent copies of the protein in the asymmetric unit. Molecular replacement was performed independently with two programs, *AMoRe* (Navaza, 2001) and *EPMR* v.2.5 (Kissinger *et al.*, 1999), in each case using diffraction data in the resolution range 3.2–15 Å. For the program *AMoRe*, the correct solution was characterized by an *R* factor and correlation coefficient of 0.502 and 0.311, respectively. The analogous values obtained during a search with the program *EPMR* were 0.537 and 0.337, respectively. The solutions obtained with the two programs were equivalent. Initial refinement was carried out with the program *CNS* (Brünger *et al.*, 1998), with 5% of the randomly selected reflections kept aside for cross-validation. After rigid-body refinement using X-ray data in the resolution range 3–15 Å, the *R* factor and $R_{\rm free}$ decreased to 0.454 and 0.473, respectively. Subsequent steps included refinement according to the simulated-annealing protocol, standard steepest-gradient minimization and refinement of *B* factors for individual atoms, interspersed with visual inspection of the electron-density maps using the programs *O* and *Xfit* (Jones *et al.*, 1991; McRee, 1999). During this process, the identity of all residues in the model was converted to match the sequence of MCP-4 and the resolution of the experimental X-ray data was extended to 2.1 Å. The resulting values of the crystallographic *R* factor and $R_{\rm free}$ were 0.278 and 0.316, respectively. Further refinement was conducted using the program *REFMAC*5.1 (Murshudov *et al.*, 1999). At this stage, the resolution was gradually extended to the limit of the experimental data (1.70 Å). The refinement was carried out employing the TLS refinement option, with each individual monomer treated as one entity. The final structure has good stereochemistry, with 94.9% and 5.1% of residues in the most favored and additionally allowed regions of the Ramachandran plot, respectively. The complete refinement statistics are shown in Table 1.

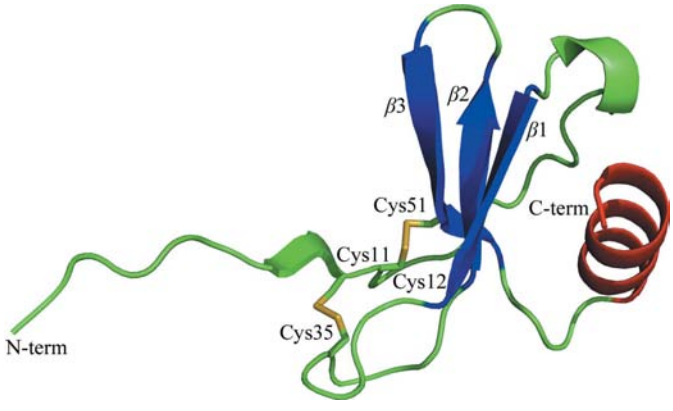

Figure 1
Cartoon representation of the MCP-4 topology. The central triple-stranded antiparallel β-sheet (β1, Lys26–Ile30; β2, Val40–Thr44; β3, Gly47–Ala52) is colored blue and the C-terminal α-helix is colored red. The two disulfide bridges (Cys11–Cys35 and Cys12–Cys51) are shown in stick representation. This figure was generated using *PyMOL* (DeLano, 2002).

3. Results and discussion

3.1. Cloning, expression, purification and characterization

Based on the previously published human MCP-4 sequence (Berkhout *et al.*, 1997), we constructed a synthetic gene encoding residues 1–75 of the mature protein and successfully expressed MCP-4 in *E. coli* with a yield of approximately 5 mg per litre of medium. Subsequently, the protein was purified from the cell lysate by a combination of cation-exchange chromatography and HPLC on a reverse-phase C-18 column. The final protein preparation was >98% pure and analytical RP-HPLC confirmed the presence of a single protein specimen (data not shown). Additionally, mass-spectrometric analysis of the final MCP-4 preparation using an Agilent Technologies 1100 LC/MSD system (Hewlett Packard) revealed that the starting methionine (a cloning artifact) had been cleaved from the protein and the newly formed N-terminus was occupied by glutamine rather than its cyclic pyroglutamate form as observed for other MCPs (Blaszczyk *et al.*, 2000).

3.2. Overview of the MCP-4 structure

The MCP-4 crystals belong to the tetragonal space group *I*4, with unit-cell parameters $a = b = 74.7$, $c = 51.6$ Å and a solvent content of 30%. The two independent MCP-4 molecules in the asymmetric unit are essentially identical and could be superimposed with an r.m.s. difference of 0.16 Å for all 65 C^{α} atoms. The final model of MCP-4, refined at 1.7 Å resolution, consists of residues Asp3–Gly67 of mature human MCP-4. In addition to protein residues, the model contained 72 waters, one molecule of trifluoroacetic acid (a residuum from the final

HPLC purification step) and six sulfate ions. Owing to the lack of interpretable electron density, the first two N-terminal residues and eight amino acids at the C-terminus could not be modeled.

The overall fold of MCP-4 is similar to the topology of other CC chemokines (Blaszczyk *et al.*, 2000; Chung *et al.*, 1995; Handel & Domaille, 1996; Lubkowski *et al.*, 1997; Meunier *et al.*, 1997). It consists of an extended N-terminal segment (Asp3–Thr10) followed by two disulfide bridges in left-handed spiral conformations (Cys11–Cys35 and Cys12–Cys51), a triple-stranded antiparallel β-sheet (β1, Lys26–Ile30; β2, Val40–Thr44; β3, Gly47–Ala52) as part of a 'Greek key' motif and an overlying C-terminal α-helix (Lys57–Gly67; Fig. 1*a*). The Cys11–Cys35 disulfide bridge couples an irregular N-terminal β-strand (amino acids Ser9–Cys11, implicated in the proposed MCP-4 dimerization) to the long hairpin loop between β1 and β2 (residues Thr31–Ala39), thus stabilizing the β-structure of MCP-4.

Although the overall fold of MCP-4 conforms to the generalized view of a chemokine tertiary structural arrangement, the superposition of available MCP structures revealed several differences documented by r.m.s. deviations of 2.8, 2.8 and 3.0 Å between corresponding C^{α} atoms of MCP-4 (amino acids Cys11–Gly67) and MCP-1 (PDB code 1dok), MCP-2 (PBD code 1esr) and MCP-3 (PDB code 1bo0), respectively. Major structural variations occur at the N-terminus of the proteins (amino acids 1–10), as well as at the hairpin loop connecting the β1 and β2 strands. Interestingly, when compared with the crystal structures of MCP-1 and MCP-2, the 'canonical' N-terminal 3_{10}-helix (amino acids Pro2–Gln6 and Asp3–Ile7 in MCP-1 and MCP-2, respectively) is absent from the MCP-4 structure (Fig. 2). However, it should be noted that in each monomer this amino-acid segment forms extensive contacts with another MCP-4 molecule within the crystal lattice, so it is not clear whether the 3_{10}-helix would exist in the apparently monomeric MCP-4 species observed *in vitro*.

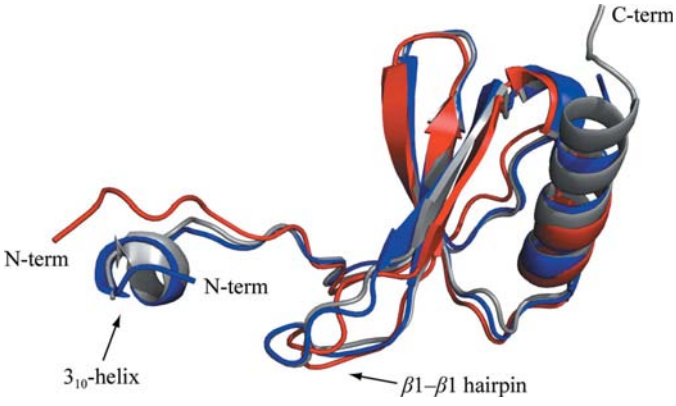

Figure 2
Superposition of MCP-1 (blue; PDB code 1dok), MCP-2 (gray; PDB code 1esr) and MCP-4 (red) crystal structures. The structures were superimposed on corresponding C^{α} atoms. Note that the N-terminal 3_{10}-helix is missing from the MCP-4 structure.

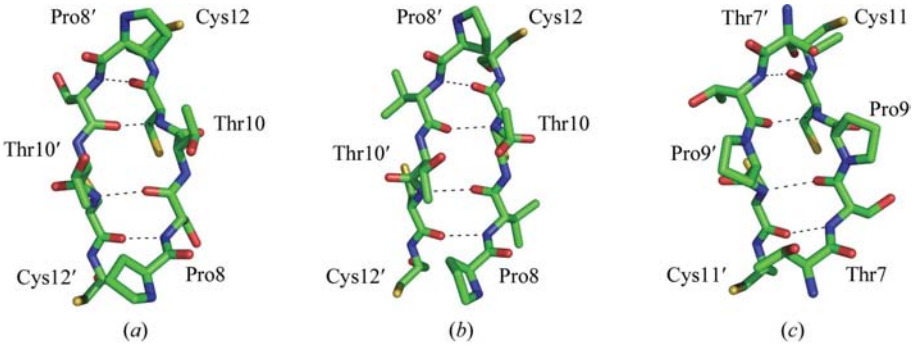

Figure 3
Dimerization 'signature' of the CC chemokine family. Formation of the antiparallel β-sheet between the N-terminal parts of two monomers contributes to the stability of the homodimers and has been observed for many CC chemokines. Amino-acid residues 8–12 (for MCP-4 and MCP-1) or 7–11 (for RANTES, also a member of the CC chemokine family with a sequence/structural similarity to MCPs) are shown in stick representation and main-chain hydrogen bonds are represented by dotted lines. (*a*) MCP-4, (*b*) MCP-1, (*c*) RANTES.

Several groups have analyzed the contribution of individual amino acids or amino-acid segments to the biological properties of MCPs (mostly MCP-1), including chemotactic activity, dimerization and interactions with GPCRs or glycosaminoglycans (Gong *et al.*, 1998; Lau *et al.*, 2004; Paavola *et al.*, 1998; Zhang *et al.*, 1994). In general, structure–function studies have consistently shown that the N-terminal region and N-terminal loop residues are essential for receptor binding, but that at the same time additional amino acids throughout the whole molecule contribute to different extents to the biological activity of MCPs. However, in the absence of structural data on GPCRs and given the overlapping specificities of MPCs, an accurate assignment of the residues determining their biological activity remains elusive.

3.3. Quaternary arrangement

Many chemokines form dimers or higher oligomers both in solution and under crystallographic conditions and oligomerization has been reported to be critical for their activity *in vivo* (Proudfoot *et al.*, 2003). MCP-1 and MCP-2 exist in an equilibrium between monomeric and dimeric forms, but MCP-4 (as well as MCP-3) is monomeric under experimental conditions *in vitro* (Crown *et al.*, 2006; Kim *et al.*, 1996). However, it is likely that higher order assemblies of the latter MCPs might be formed *in vivo*, especially in the presence of glycosaminoglycans on endothelial cell surfaces or within the extracellular matrix (Lau *et al.*, 2004; Proudfoot *et al.*, 2003). Furthermore, MCP-4 readily forms heterodimers with other MCP-family members, suggesting the existence of common structural motifs involved in oligomer formation (Crown *et al.*, 2006).

Our final model contains two independent MCP-4 monomers in the asymmetric unit and their spatial arrangement suggests that they could represent an MCP-4 biological dimer.

The MCP-4 dimer interface, with a total buried surface area of approximately 1230 Å^2, features both hydrophobic and polar interactions. The main-chain amides of Ala4 and Asn6 form hydrogen bonds to the hydroxyl groups of the side chains of Ser16 (3.2 Å) and Ser17 (2.8 Å), respectively. The Ala4 carbonyl O atom accepts hydrogen bonds from the main-chain amides of Ser17 (3.1 Å) and Lys18 (3.3 Å), while the carbonyl O atom of Asn6 interacts with the Cys51 amide (2.9 Å) and the Ser16 O$^{\gamma}$ group (3.3 Å). Additionally, the side-chain carbonyl of Asn6 is within hydrogen-bonding distance of Thr14 OG1 (2.8 Å) and the Arg34 guanidinium group hydrogen bonds to the Phe13 main-chain carbonyl (3.1 Å). The set of polar interactions is complemented by a hydrogen-bonding network within the two-stranded antiparallel β-sheet involving residues Ser9–Cys11 of both MCP-4 monomers (Fig. 3). The latter feature is well conserved at the inter-monomer interfaces of CC chemokines and could thus be regarded as a structural signature of the dimerization motif of the CC chemokine family (Blaszczyk *et al.*, 2000; Chung *et al.*, 1995; Lubkowski *et al.*, 1997).

Nonpolar contacts are represented by the interaction of the Leu5 side chain with the hydrophobic pocket shaped by the side chains of Lys18, Ile20 and Ile50. Similarly, Pro8 is buried in the pocket defined by the side chains of Thr10, Ile41 and Glu49 and the disulfide bridge between Cys12 and Cys51 (Fig. 4). It is interesting to note that Pro8 is conserved in both MCP-1 and MCP-2, which readily form higher oligomers, while it is substituted by serine in the monomeric MCP-3. Additionally, mutagenesis studies revealed that a substitution of Pro8 by alanine in MCP-1 abolishes its dimerization *in vitro* and its biological activity *in vivo* (Paavola *et al.*, 1998; Proudfoot *et al.*, 2003). The above-mentioned arrangement of MCP-4 monomers is reminiscent of the dimerization interfaces of human MCP-1 and MCP-2, thus supporting biochemical evidence for heterooligomerization between different MCP molecules (Crown *et al.*, 2006).

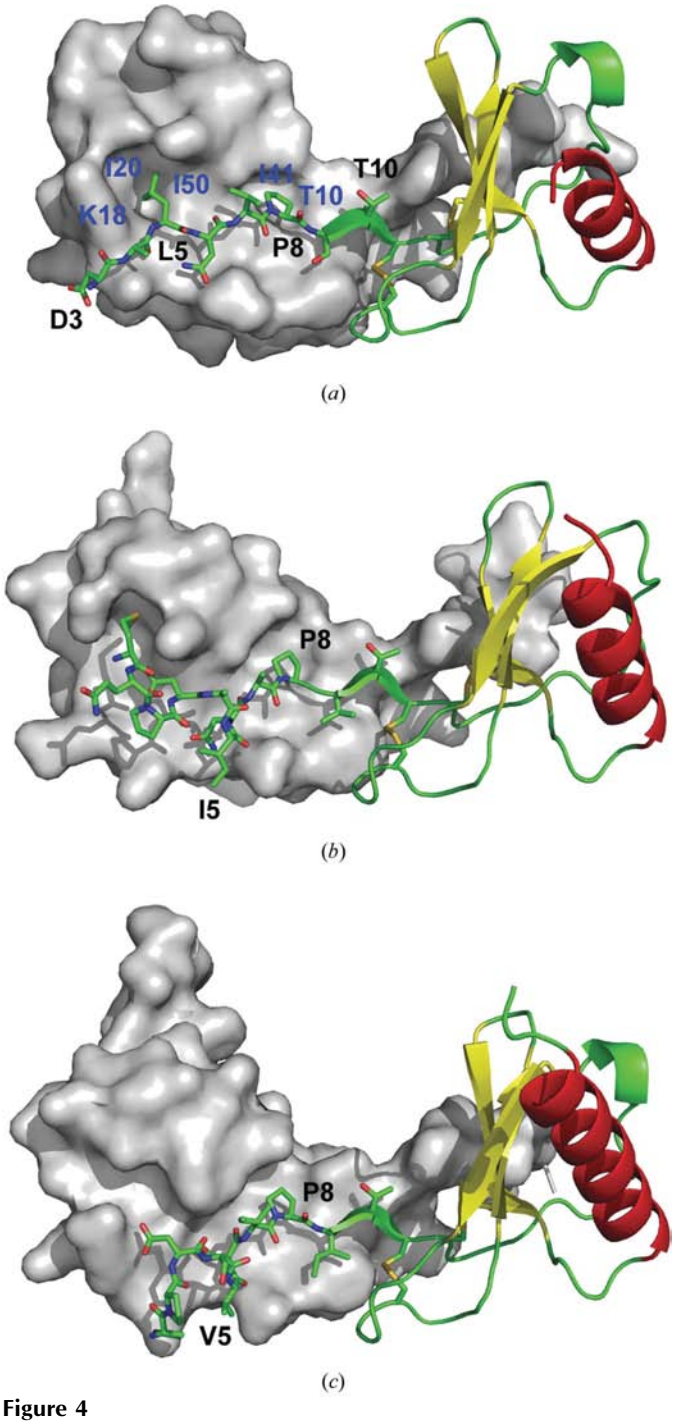

Figure 4
Dimer interfaces of MCP-4, MCP-1 and MCP-2. (*a*) The putative MCP-4 dimer as observed in the asymmetric unit. (*b*) The MCP-1 dimer as observed in the asymmetric unit (PDB code 1dok). (*c*) The MCP-2 dimer generated by a crystallographic symmetry operation (from Blaszczyk *et al.*, 2000; PDB code 1esr). One of the monomers is shown in surface representation, while the second monomer is visualized by a combination of stick and cartoon representations. Residues of the first monomer forming hydrophobic pockets (surface representation) are indicated with blue labels; the residues of the second monomer are labeled in black.

We acknowledge the use of beamline 22-ID of the South-east Regional Collaborative Access Team (SER-CAT), located at the Advanced Photon Source (APS), Argonne National Laboratory, Argonne, Illinois. Use of the APS was supported by the US Department of Energy, Office of Science, Office of Basic Energy Sciences under Contract No. W-31-109-Eng-38. The project was supported by the Intramural Research Program of the NIH, National Cancer Institute, Center for Cancer Research.

References

Berkhout, T. A. *et al.* (1997). *J. Biol. Chem.* **272**, 16404–16413.
Blaszczyk, J., Van Coillie, E., Proost, P., Van Damme, J., Opdenakker, G., Bujacz, G. D., Wang, J. M. & Ji, X. (2000). *Biochemistry*, **39**, 14075–14081.
Brünger, A. T., Adams, P. D., Clore, G. M., DeLano, W. L., Gros, P., Grosse-Kunstleve, R. W., Jiang, J.-S., Kuszewski, J., Nilges, M., Pannu, N. S., Read, R. J., Rice, L. M., Simonson, T. & Warren, G. L. (1998). *Acta Cryst.* D**54**, 905–921.
Charo, I. F. & Taubman, M. B. (2004). *Circ. Res.* **95**, 858–866.
Chung, C. W., Cooke, R. M., Proudfoot, A. E. & Wells, T. N. (1995). *Biochemistry*, **34**, 9307–9314.
Craig, M. J. & Loberg, R. D. (2006). *Cancer Metastasis Rev.* **25**, 611–619.

Crown, S. E., Yu, Y., Sweeney, M. D., Leary, J. A. & Handel, T. M. (2006). *J. Biol. Chem.* **281**, 25438–25446.
DeLano, W. L. (2002). *The PyMOL Molecular Visualization System.* DeLano Scientific, San Carlos, USA. http://www.pymol.org.
Gong, J. H. & Clark-Lewis, I. (1995). *J. Exp. Med.* **181**, 631–640.
Gong, W., Howard, O. M., Turpin, J. A., Grimm, M. C., Ueda, H., Gray, P. W., Raport, C. J., Oppenheim, J. J. & Wang, J. M. (1998). *J. Biol. Chem.* **273**, 4289–4292.
Handel, T. M. & Domaille, P. J. (1996). *Biochemistry*, **35**, 6569–6584.
Hoover, D. M. & Lubkowski, J. (2002). *Nucleic Acids Res.* **30**, e43.
Jones, T. A., Zou, J.-Y., Cowan, S. W. & Kjeldgaard, M. (1991). *Acta Cryst.* A**47**, 110–119.
Kim, K. S., Rajarathnam, K., Clark-Lewis, I. & Sykes, B. D. (1996). *FEBS Lett.* **395**, 277–282.
Kissinger, C. R., Gehlhaar, D. K. & Fogel, D. B. (1999). *Acta Cryst.* D**55**, 484–491.
Lau, E. K., Paavola, C. D., Johnson, Z., Gaudry, J. P., Geretti, E., Borlat, F., Kungl, A. J., Proudfoot, A. E. & Handel, T. M. (2004). *J. Biol. Chem.* **279**, 22294–22305.
Leach, K., Charlton, S. J. & Strange, P. G. (2007). *Biochem. Pharmacol.* **74**, 881–890.
Lubkowski, J., Bujacz, G., Boque, L., Domaille, P. J., Handel, T. M. & Wlodawer, A. (1997). *Nature Struct. Biol.* **4**, 64–69.
Luster, A. D. (1998). *N. Engl. J. Med.* **338**, 436–445.
McRee, D. E. (1999). *J. Struct. Biol.* **125**, 156–165.
Masure, S., Paemen, L., Proost, P., Van Damme, J. & Opdenakker, G. (1995). *J. Interferon Cytokine Res.* **15**, 955–963.
Meunier, S., Bernassau, J. M., Guillemot, J. C., Ferrara, P. & Darbon, H. (1997). *Biochemistry*, **36**, 4412–4422.
Murshudov, G. N., Vagin, A. A., Lebedev, A., Wilson, K. S. & Dodson, E. J. (1999). *Acta Cryst.* D**55**, 247–255.
Navaza, J. (2001). *Acta Cryst.* D**57**, 1367–1372.
Otwinowski, Z. & Minor, W. (1997). *Methods Enzymol.* **276**, 307–326.
Paavola, C. D., Hemmerich, S., Grunberger, D., Polsky, I., Bloom, A., Freedman, R., Mulkins, M., Bhakta, S., McCarley, D., Wiesent, L., Wong, B., Jarnagin, K. & Handel, T. M. (1998). *J. Biol. Chem.* **273**, 33157–33165.
Proost, P., Wuyts, A. & Van Damme, J. (1996). *J. Leukoc. Biol.* **59**, 67–74.
Proudfoot, A. E. (2002). *Nature Rev. Immunol.* **2**, 106–115.
Proudfoot, A. E., Handel, T. M., Johnson, Z., Lau, E. K., LiWang, P., Clark-Lewis, I., Borlat, F., Wells, T. N. & Kosco-Vilbois, M. H. (2003). *Proc. Natl Acad. Sci. USA*, **100**, 1885–1890.
Rollins, B. J. (1997). *Blood*, **90**, 909–928.
Romagnani, S. (2002). *Mol. Immunol.* **38**, 881–885.
Westby, M. & van der Ryst, E. (2005). *Antivir. Chem. Chemother.* **16**, 339–354.
Xia, Y. & Frangogiannis, N. G. (2007). *Inflamm. Allergy Drug Targets*, **6**, 101–107.
Zhang, Y. J., Rutledge, B. J. & Rollins, B. J. (1994). *J. Biol. Chem.* **269**, 15918–15924.
Zlotnik, A. & Yoshie, O. (2000). *Immunity*, **12**, 121–127.